

Multi-Task Learning by a Top-Down Control Network

Hila Levi¹ Shimon Ullman¹

Abstract

A general problem that received considerable recent attention is how to perform multiple tasks in the same network, maximizing both prediction accuracy and efficiency of training. Recent approaches address this problem by branching networks, or by a channel-wise modulation of the feature-maps with task specific vectors. We propose a novel architecture that uses a top-down network to modify the main network according to the task in a channel-wise, as well as spatial-wise, image-dependent computation scheme. We show the effectiveness of our scheme by achieving better results than alternative state-of-the-art approaches to multi-task learning. We also demonstrate our advantages in terms of task selectivity, scaling the number of tasks, learning from fewer examples and interpretability.

1. Introduction

The goal of multi-task learning is to improve the learning efficiency and increase the prediction accuracy of multiple tasks learned and performed in a shared network.

In recent years, several types of architectures have been proposed to combine multiple tasks training and evaluation. Most current schemes assume task-specific branches, on top of a shared backbone (Figure 1a) and use a weighted sum of tasks losses for training (Chen et al., 2017; Kendall et al., 2018; Sener & Koltun, 2018). Having a shared representation is more efficient from the standpoint of memory and sample complexity (Zhao et al., 2018). However, the performance of the multi-branch architecture is highly dependent on the relative losses weights and the task correlations, and cannot be easily determined without a "trial and error" phase search (Kendall et al., 2018).

Another type of architecture proposed recently (Zhao et al.,

¹Department of Computer Science, Weizmann Institute, Rehovot, Israel. Correspondence to: Hila Levi <hila.levi@weizmann.ac.il>, Shimon Ullman <shimon.ullman@weizmann.ac.il>.

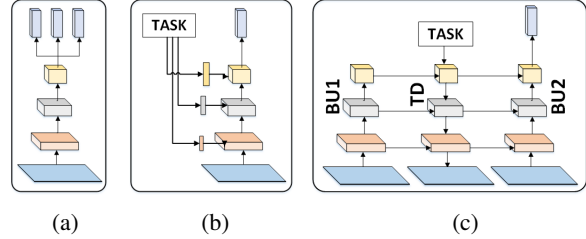


Figure 1. (a) Multi branched architecture, task-specific branches on a top of a shared backbone. (b) Channel-wise modulation architecture, uses task-embedding to modulate the feature maps along the main network (c) **Our architecture, a top-down (TD) control network:** image information, extracted by the BU1 stream, is accumulated by the TD stream, and affects the control of the featuremaps along the BU2 stream according to the current task.

2018; Strezoski et al., 2019) uses task-specific vectors to modulate the feature-maps along a feed-forward network, in a channel-wise manner (figure 1b). Channel-wise modulation based architecture has been shown to decrease the destructive interference between conflicting gradients of different tasks (Zhao et al., 2018) and allowed Strezoski et al. (2019) to scale the number of tasks (up to 312) without changing the network. Here, both training and evaluation use the single tasking paradigm: executing one task at a time, rather than getting all the task responses in a single forward pass. Executing one task at a time is also possible by integrating task-specific modules along the network (Maninis et al., 2019). A limitation of using task-specific modules or of using a fixed number of branches, is that it may become difficult to add additional tasks at a later time during the system life-time.

We propose a new type of architecture with no branching, which performs a single task at a time with no task-specific modules (Figure 1c). The core component of our approach is a top-down (TD) network, which controls individual units within a tensor. It uses task information, combined with image information, obtained from a first bottom-up (BU1) network, and modifies a second bottom-up (BU2) network, which is common for all the tasks. In our approach, the modification is not only channel-wise but also spatial-wise, by a full tensor modification, calculated along the TD stream and allowing attention to specific locations in the image (as

in figure 2a). In contrast to previous works, this approach is also "image-aware" in the sense that image information, extracted by the BU1 stream, is accumulated by the TD stream, and affects the control of the featuremaps along BU2 (useful for the tasks in figures 2b and 2c). As shown later, the task control by the TD component becomes highly efficient in the sense that the network becomes more specifically tuned to the selected task compared with alternatives.

We empirically evaluated the proposed approach on three different datasets. First, we demonstrate better accuracy compares with all other approaches on MultiMNIST which increases with the number of tasks and is obtained across multiple model sizes. We introduce a task specificity test, showing that our architecture achieves higher task specificity than the channel-modulation architecture. Second, we show improved results and faster dynamics while scaling up the number of tasks to 1645 on the CLEVR (Johnson et al., 2017) dataset. Third, we outperformed all baselines and demonstrated our inherent attention mechanism on the CUB-200 (Welinder et al., 2010) dataset. The results demonstrate the advantages of our scheme in terms of both accuracy and effective learning. The advantages may be explained, at least in part, by the higher task specificity of our method.

2. Related Work

Our work draw ideas from the following research lines:

Multiple Task Learning (MTL) Multi task learning has been used in machine learning well before the revival of deep networks (Caruana, 1997). The success of deep neural networks in single task performance (e.g. in classification, detection and segmentation) has renewed the interests of the computer vision community in the field (Kokkinos, 2017; He et al., 2017; Redmon & Farhadi, 2017). Although our primary application area is computer vision, multi task learning has also many application in other fields like natural language processing (Hashimoto et al., 2016; Collobert & Weston, 2008) and even across modalities (Bilen & Vedaldi, 2016). We further refer the interested reader to a review that summarizes recent work in the field (Ruder, 2017).

Over the years, several types of architectures have been proposed in computer vision to combine the training and evaluation of multiple tasks. First works used several duplications (as many as the tasks) of the base network, with connections between them to pass useful information between the tasks (Misra et al., 2016; Rusu et al., 2016). These works do not share computations and cannot scale with the tasks. More recent architectures, which are in common practice these days, assume task-specific branches on a top of a shared backbone, and use a weighted sum of losses to train them. The joint learning of several tasks has proven to be beneficial in several cases (He et al., 2017) but can also

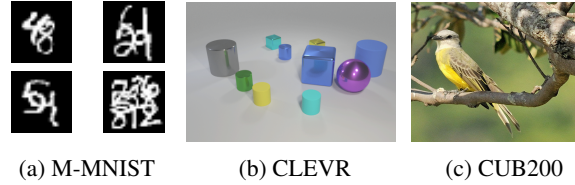


Figure 2. Images examples with their corresponding tasks. (a) M-MNIST examples, the tasks are to recognize the digits by their location. (b) CLEVR dataset, an example task is to recognize the material of the cylinder to the right of the blue cube. (c) CUB200 dataset, an example task is to identify the color of the bird’s neck.

decrease the results of some of the tasks due to a limited network capacity, uncorrelated gradients from the different tasks (sometimes called destructive inference) and different learning rates (Kirillov et al., 2019). A naive implementation of multi-task learning requires careful calibration of relative losses of the different tasks. To address these problem several methods have been proposed: "Grad norm" (Chen et al., 2017) dynamically tunes gradients magnitudes over time, to obtain similar learning rates of the different tasks. Kendall et al. (2018) uses a joint likelihood formulation to derive task weights based on the intrinsic uncertainty in each task. Sener & Koltun (2018) applies an adaptive weighting of the different tasks, to force a pareto optimal solution to the multi task problem.

Along an orthogonal line of research, other works suggested to add task-specific modules to be activated or deactivated during training and evaluation, depending on the task at hand. Liu et al. (2019b) suggests task specific attention networks in parallel to a shared recognition network. Maninis et al. (2019) suggests adding several types of low-weight task-specific modules (e.g. residual convolutional layers, squeeze and excitation (SE) blocks and batch normalization layers) along the recognition network. Note that the SE block essentially creates a modulation vector, to be channel-wise multiplied with a feature-map. Modulation vectors have been further used in Strezoski et al. (2019) for a recognition application, in Cheung et al. (2019) for continual learning applications and in Zhao et al. (2018) for a retrieval application and proved to decrease the destructive interference between tasks and the effect of the catastrophic forgetting phenomena.

Our design, in contrast, does not use multi-branch architecture, nor task-specific modules. Our network is fully-shared between the different tasks. Compared to Zhao et al. (2018), we modulate the feature-maps in the recognition network channel-wise as well as spatial-wise, depending on both the task and the specific image at hand.

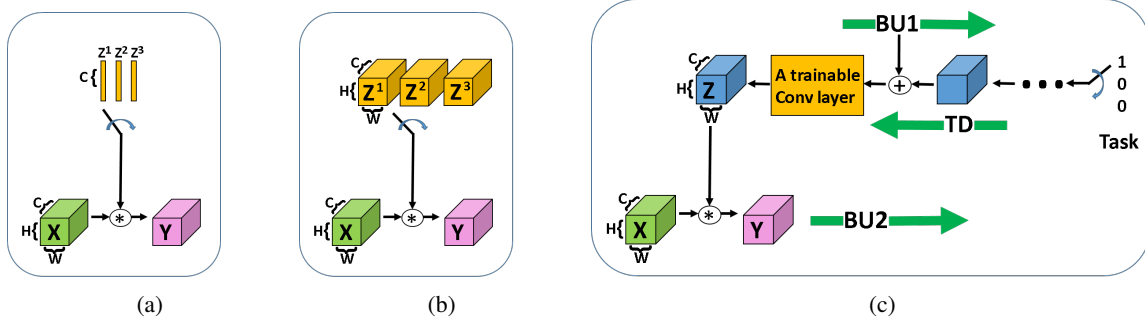


Figure 3. Several types of modulation modules, the trainable parameters are illustrated in yellow. For simplicity we show only one modulation stage, where \mathbf{X} is the input tensor and \mathbf{Y} is the output tensor. (a) task-dependent channel-modulation architecture, the modulation vectors are switched by the task and explicitly being optimized. (b) Hypothetical extension of (a) to spatial-wise modulation tensors, cannot be done in practice due to the huge number of parameters to optimize. (c) **Our approach:** We optimize the parameters in the convolutional layers along the top-down network and use the created featuremaps to modify the activations in the main network.

Top-Down Modulation Networks Neuroscience research provides evidence for a top-down context, feedback and lateral processing in the primate visual pathway (Gazzaley & Nobre, 2012; Gilbert & Sigman, 2007; Lamme et al., 1998; Hopfinger et al., 2000; Piëch et al., 2013; Zanto et al., 2010) where top-down signals modulate the neural activity of neurons in lower-order sensory or motor areas based on the current goals. This may involve enhancement of task-relevant representations or suppression for task-irrelevant representations. This mechanism underlies humans ability to focus attention on task-relevant stimuli and ignore irrelevant distractions (Hopfinger et al., 2000; Piëch et al., 2013; Zanto et al., 2010).

In this work, consistent with this general scheme, we suggest a model that uses top-down modulation in the scope of multi-task learning. Top down modulation networks with feedback, implemented as conv-nets, have been suggested by the computer vision community for some high level tasks (e.g. re-classification (Cao et al., 2015), keypoints detection (Carreira et al., 2016; Newell et al., 2016), crowd counting (Sam & Babu, 2018), curriculum learning (Zamir et al., 2017) etc.) and here we apply them to multi-task learning applications.

3. Approach

We will first describe the task-dependent vector-modulation mechanism, as proposed in Zhao et al. (2018), illustrated in figure 3a, then describe our architecture (figure 3c) in detail.

3.1. Vector-Modulation Module

A vector-modulation (a channel-wise modulation) of a given tensor \mathbf{X} by a vector z is defined as the product of the elements of the vector z and the corresponding channels of the tensor \mathbf{X} . Each element in the output tensor \mathbf{Y} is

calculated by:

$$\mathbf{Y}(y, x, ch) = \mathbf{X}(y, x, ch) * z(ch) \quad (1)$$

where \mathbf{X} is the tensor to be modulated and \mathbf{Y} is the modulated tensor, both in the form $(H \times W \times C)$ where H , W , are the spatial dimensions of the tensors and C their channel dimension. The vector $z \in \mathbb{R}^C$ has dimension equal to the number of channels of \mathbf{X} , \mathbf{Y} . x, y, ch are the column, row, and channel number and indicate a specific element in a tensor. In training the network, the elements of z are considered as parameters and are directly optimized (C additional parameters).

In the scope of Multi Task Learning, where several tasks co-exist, the network switches on the fly between several modulation vectors $\{z^k\}_{k=1}^K$ where K is the number of tasks, see figure 3a for illustration. The network performs one task at a time, and the modulated tensor \mathbf{Y} depends on the selected task. This vector-modulation module has been used in Zhao et al. (2018) separately for every stage in the recognition network (with additional CK parameters in every stage).

Two limitations of this module are that it ignores the spatial dimensions of the image, and the lack of information from the image itself. The possible use of the same strategy to explicitly optimize spatial-aware modulation tensors $\{\mathbf{Z}^k(y, x, ch)\}_{k=1}^K$ (figure 3b) was discussed in Zhao et al. (2018) but was deemed infeasible due to the large amount of added parameters ($HWCK$ additional parameters in every stage). Our method addresses both of these issues in an efficient manner and demonstrates better accuracy, showing that spatial-wise modulation and the use of image information are beneficial to many kinds of tasks.

3.2. Top-Down Tensor-Modification Module

A tensor modification is defined by:

$$\mathbf{Y}(y, x, ch) = \mathbf{X}(y, x, ch) * \mathbf{Z}(y, x, ch) \quad (2)$$

Where $\mathbf{Z} \in \mathbb{R}^{H \times W \times C}$ is a modification tensor.

To avoid the infeasible computation of directly optimizing \mathbf{Z} , we propose the use of created featuremaps as the modification tensors. Practically, we use a dedicated top-down (TD) convolutional stream, shared between the tasks, to create the modification featuremaps, and optimize the weights of the convolutional layers instead of directly optimizing the modification tensors (figure 3c). The number of added parameters in this case depends on the precise architecture of the TD stream but can be approximately estimated by $3 \times 3 \times C^2$ parameters for each convolutional layer (several convolutional layers may be used in one stage). Avoiding the dependency of the number of added parameters on H, W and K allows us to apply the proposed architecture to large images and to scale the number of tasks, as illustrated our experiments.

3.3. Image-Aware Task-Dependent Top-Down Control Network

An illustration of our network design is shown in figure 1c. In our design, a bottom-up (BU2) recognition network is modified by the featuremaps along a top-down (TD) stream. The inputs to the TD stream are the current task k , and the feature-maps along the first bottom-up stream (BU1, where BU1 and BU2 share the same weights), added to the TD stream via lateral connections. The outputs of the TD stream are its feature-maps, which integrate image, content and task information in a multi-scale manner and sequentially control the individual units in the tensors along the main recognition network (BU2).

Figure 3c illustrate our architecture for one modification step.

Top-Down structure In most of our experiments, unless stated otherwise, we use a fixed standard implementation and implement the TD stream as a replica of the BU stream in terms of number of layers, type of layers and number of channels in each layer. Further work on multi-task networks may lead to changes in this architecture choice.

Auxiliary losses Our architecture can be naturally decomposed into three sub-networks (BU1, TD, BU2), allowing the structural advantage of adding auxiliary losses at the end of the BU1 or TD streams. This possibility is application-dependent. In the scope of multi-task learning, the TD auxiliary loss might be beneficial because it allows the use

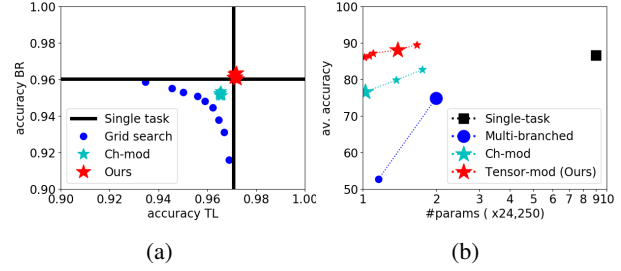


Figure 4. (a) **Multi-MNIST accuracy plot**, The two axes are the accuracies of the two tasks, top-right is better. We show higher accuracies than the single-task baseline, while using fewer parameters. (b) **Comparison of four architectures by average accuracy vs. model size** in the M-MNIST 9-classes experiment, top-left is better. Our approach shows better performance on different model sizes compared with alternative architectures.

of spatial information in a task-dependent manner. This issue is further discussed in sections 4.3.3 and 4.3.4 where we demonstrate the use of a localization loss in the last TD featuremap. Applying the localization loss in train time allows us to obtain an attention map in inference time, which illustrates the relative weights assigned by the network to different locations in the image.

4. Databases and Experiments

4.1. Databases

We validated our approach on three different datasets:

MultiMNIST MultiMNIST (Sabour et al., 2017) is a multi-task learning version of the MNIST dataset in which multiple MNIST images are placed on the same image. We use 2, 4 and 9 classes experiments built as suggested by Sener & Koltun (2018). Several examples are demonstrated in Figure 2a. In the 2-classes experiment the tasks are: classifying the digit on the top-left (task-TL) and classifying the digit on the bottom-right (task-BR). We correspondently add tasks (TM, TR, L, C, R, BL and BM) for classifying the digits on the top-mid, top-right, left, center, right, bottom-left and bottom-mid on the 4 and 9-classes experiments. The digits in each position are independently chosen. We use 60K examples and directly apply LeNet (LeCun et al., 1998) as the underlying backbone in our experiments.

CLEVR CLEVR is a synthetic dataset, consists of 70K training images and 15K validation images, mainly used as a diagnostic dataset for VQA. The dataset includes images of 3D primitives, with multiple attributes (shape, size, color and material) and a set of corresponding (question-answer) tuples. We followed the work Liu et al. (2019a), which suggested to use CLEVR not as a VQA dataset, but rather

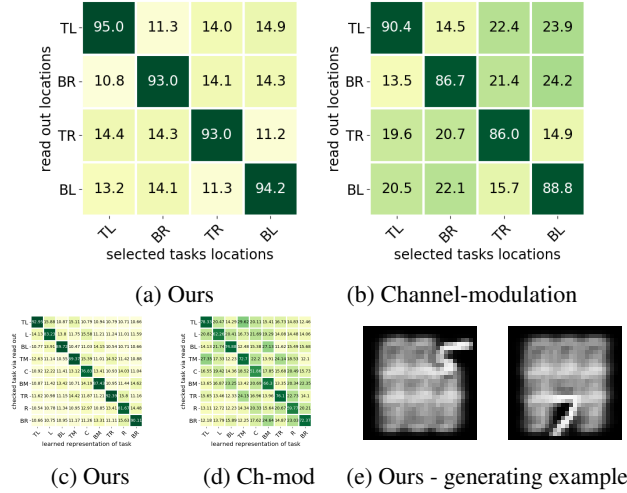


Figure 5. Task selectivity. The columns in each plot are the selected task locations, the rows are the readout locations. With high selectivity, off-diagonal recognition will be at chance level. (a,b) Our scheme shows higher selectivity than the channel-modulation scheme. (c,d) Similar results on the 9-classes experiment. (e) task-selectivity visualizations: reconstructing the image from the output layer (see supplementary materials).

as a referring expression dataset, and further adapt it to a multi-task learning methodology. The tasks in our setup consist of 40 query-attribute questions, randomly chosen from the dataset questions with program length smaller than six. A typical question / task in this set (set A) is: "What is the color of the metal cylinder?". Another set (set B) of 160 tasks was built with respect to set A by query the attributes of an object that is to the (left, right, up, down) of the described object ("What is the color of the object to the right of the metal cylinder?"). To demonstrate our ability to scale the number of tasks, set B was further extended to include all the possible questions (1645 tasks) in the described structure. Both sets are further discussed in the Supplementary materials.

CUB200 is a fine grained recognition dataset that provides 11,788 bird images (equally divided for training and testing) over 200 bird species with 312 binary attribute annotations, most of them referring to the colors of specific birds' parts. In contrast to other work (Strezoski et al., 2019) that used all the 312 attributes as yes/no questions, we re-organized the attributes as a multi-task problem of 12 tasks (for 12 annotated bird's parts) each with 16 classes (the annotated colors + an unknown class) and trained using a multi-class cross-entropy loss. To demonstrate our interpretability capability, we further used the parts' location, annotated by a single point to each seen part, as an auxiliary target at the end of the TD stream.

Table 1. Performance (mean of 5 repetitions) on Multi-MNIST. Our architecture consistently achieves highest accuracies.

	ALG	#Params	Av. Acc
2 tasks	Single task	x2	96.46
	Uniform scaling	x1.12	95.30
	mult-obj-opt	x1.12	95.81
	ch-mod	x1.002	95.87
	Ours	x1.29	96.67
4 tasks	Single task	x4	94.15
	Uniform scaling	x1.37	90.71
	mult-obj-opt	x1.37	91.24
	ch-mod	x1.007	91.38
	Ours	x1.32	94.64
9 tasks	Single task	x9	86.62
	Uniform scaling	x1.99	74.80
	mult-obj-opt	x1.99	75.13
	ch-mod	x1.015	76.56
	ch-mod (ext)	x1.37	79.81
	Ours	x1.39	88.07

4.2. Experiments

architecture We use LeNet, VGG-11 and resnet-18 as our backbone BU architectures for the Multi-MNIST, CLEVR and CUB-200 experiments correspondingly. Each of the backbones has been divided to two parts; a first part that consists mainly of the convolutional layers of the backbone and a second part with the fully connected layers (the classifier).

In our architecture, both BU streams consist of the first part of the backbone and share their weights. The TD stream, unless specified otherwise, is a replica of the BU stream, in terms of layers structure and number of channels, combined with bilinear upsampling layers. The classifier is only attached to the BU2 stream. Information is passed between the BU1, TD and BU2 streams using lateral connections implemented as 1x1 convolutions. A task embedding layer (a fully connected layer) is added on the top of the TD stream. See an illustration of the full scheme in figure 1c and a detailed architecture description of the Multi-MNIST experiments in the supplementary materials.

baselines We compare our method with a "single task" approach, where each task is solved by its own network, with a "uni-scale" (uniform scaling, sometimes called multi-branched) approach, where an equally weighted sum of the individual losses is being minimized, with a "mult-obj-opt" (multi objective optimization) approach where the weights are dynamically tuned as in Sener & Koltun (2018) and with "ch-mod", a channel-wised vector modulation architecture (Zhao et al., 2018).

Table 2. Ablations on Multi-MNIST: adding spatial-wise and image-aware components

ALG	image	spatial	TL accuracy	BR accuracy	BL accuracy	TR accuracy	↑ mean
ch-mod	×	×	93.29 \pm 0.17	90.05 \pm 0.38	90.09 \pm 0.18	92.11 \pm 0.27	0
–	✓	×	93.52 \pm 0.18	90.62 \pm 0.21	90.64 \pm 0.18	92.39 \pm 0.16	+0.41
–	×	✓	95.45 \pm 0.11	93.29 \pm 0.17	93.19 \pm 0.24	94.60 \pm 0.15	+2.75
Ours	✓	✓	95.76 \pm 0.07	93.89 \pm 0.29	93.81 \pm 0.27	95.11 \pm 0.10	+3.26

4.3. Results

We start with a simple network with limited capacity, and compare the different approaches (multi-branch, channel modulation, ours) in terms of performance.

4.3.1. MULTIMNIST

We use the Multi-MNIST dataset to demonstrate our performance for 2, 4, and 9 tasks recognition problems. All models trained using a standard LeNet architecture. We used a batch size of 512 images trained on 1 GPU with learning rate of $1e^{-3}$ using the Adam optimizer. We followed Sener & Koltun (2018) and decrease the learning rate by a factor of 2 every 30 epochs. For a fair comparison, all models were trained with the same amount of training examples per task (60K examples per task in an epoch) for 100 epochs.

Figure 4a shows the performance of the 2-classes experiment as a plot of accuracies on task-TL and task-BR for the single task approach (vertical and horizontal lines correspondingly) and the multi-branched approach for different mixes loss weights (the blue dots). The plot demonstrates a capacity problem, where better accuracies in one task cannot be achieved without being reflected as lower accuracies on another task. Our results (5 independent experiments) are marked as a red star, showing better accuracies than the single-task case with fewer parameters. Modulating the recognition stream channel-wise only (cyan stars) achieves lower results.

Table 1 summarizes our results on the Multi-MNIST experiment while using 2, 4 and 9 tasks. We show the average accuracy of all tasks based on 5 experiments for each row. The third column shows the number of parameters as a multiplier of the number of parameter in a standard Lenet architecture. Detailed results for each task with standard deviation over 5 experiments and an exact calculation of the number of parameters are specified in the supplementary materials. Our method achieves significantly better results than all the other approaches, even compared to the single-task baseline. Scaling the number of tasks increases the accuracy gap almost without additional parameters. Extending the channel-modulation scheme to a wider backbone ("ch-mod(ext)" in the table, with 15 and 25 channels fea-

turemaps) with roughly the same number of parameters as in our scheme, keeps a large accuracy gap.

Figure 4b demonstrates the average accuracy of the 9-classes experiment as a function of the number of parameters in four types of architectures. Large markers correspond to the fixed architectures used in the experiments. Small markers correspond to wider LeNet architectures or to reduced TD implementations (using TD streams with 1, 4 or 6 channels along its featuremaps). exact design choices are summarized in the supplementary materials. Our family of architectures corresponds to the highest curve in the plot.

4.3.2. ABLATIONS & COMPARISONS ON MULTI-MNIST

We further conducted ablation studies on Multi-MNIST, to examine several aspects of our proposed architecture.

Spatial-wise & image-aware modification modules. Our experiments show that extending the existing channel-wise modulation architecture to our architecture (which is also image-aware and spatial-wise) improves the results. Table 2 quantify the improvement in the results compared to the channel-wise baseline (first row in the table). We show *mean* \pm *std* based on 5 repetitions for each row. Using a channel-wise image-aware architecture by sequentially integrating information from average pooling vectors of the featuremaps in BU1 (second row) improves the accuracies by $\sim 0.4\%$. Using a spatial-wise TD modification without using the information from BU1 stream (third row) improve the accuracies by $\sim 2.7\%$. Our approach, that uses both image-aware and spatial-wise information sources, improves the accuracy by a solid gap of $\sim 3.3\%$.

Tasks selectivity. To test the selectivity of the representations produced by the BU2 stream we tried to predict not only the selected task but the digits in all four locations. For this purpose following training we attached four read-out branches (two layers each) to the top layer of BU2 and trained each one to predict one of the locations. The prediction accuracies, conditioned by the 4 tasks, are summarized in figure 5a. The results show over 90% accuracy for the task location branch and close to chance-level accuracies for all other branches. Performing the same experiment on the top of BU1 produces accuracies in the range of (30%, 40%) for all branches. Figure 5b summarizes the results of the

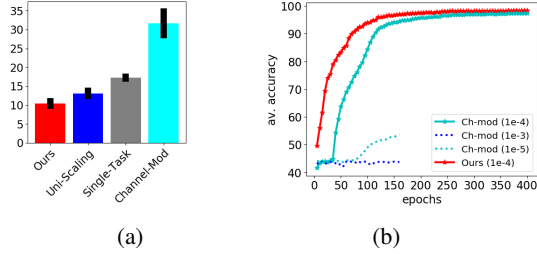


Figure 6. **Training dynamics:** (a) the number of presented examples (x60K) required to reach a fixed accuracy level on Multi-MNIST. Our architecture reach the target accuracy with a lower number of training examples than any of the alternative methods. (b) training curves on CLEVR, 1645 tasks, set B. Our architecture achieves higher accuracies while demonstrating faster dynamics. Dotted curves - optimizing the learning rates (see text).

same experiment for the channel modulation architecture, which show less selectivity. Additional results are given in the supplementary materials.

Training dynamics. Figure 6a shows the number of presented examples (unlike presented examples per task used earlier) needed for the different approaches to reach a certain accuracy level (90% of the final accuracy of our approach) in the 4-classes setup. We show mean \pm std based on 10 independent experiments. Our approach reaches the target accuracy much faster than any of the alternative methods, even with a fixed budget of training examples (while each task sees 4 times less training examples than the uniform scaling approach). The channel-modulation approach training dynamics are much slower. Following these results, in all following experiments, we used the same amount of presented examples per epoch for all of the architectures, meaning less examples per task for our scheme.

4.3.3. CLEVR

We used the CLEVR dataset to test performance and training dynamics while scaling the number of tasks (up to 1645) and increasing the tasks difficulty (using different sets of tasks) with a fixed model size.

As previously discussed, we used two sets of tasks: set A with relatively simple query-attribute tasks (used in ten / forty tasks setups) and set B with more difficult query-attribute tasks (used in 40 / 80 / 160 / 1645 tasks setups). We trained all models using a VGG-11 architecture but decreased the number of channels in the output of the last convolutional layer from 512 to 128 to allow training with larger batch size. An auxiliary localization loss was added to the architectures, indicated with \checkmark on the second column of table 3. A detailed analysis of the number of parameters and the architectures can be found in the supplementary

Table 3. Performance on CLEVR, higher is better. All architectures trained for 100 epochs. Our approach yields better accuracies compared to the alternatives with a larger gap on set B, characterized with more difficult tasks.

ALG	loc	#P	set A	#P	set B
Single task	\times	x10	99.81	x40	\times
uni-sc	\times	x6.01	99.63	x21.03	68.10
uni-sc	\checkmark	x6.01	99.88	x21.04	73.82
ch-mod	\times	x1.001	99.57	x1.002	86.91
ch-mod	\checkmark	x1.001	99.75	x1.003	89.97
Ours	\checkmark	x1.56	99.91	x1.56	96.85

Table 4. Performance on CLEVR, set B, trained for 100 epochs. Our approach is scalable with the number of tasks and uses almost no additional parameters as tasks are added.

	40 tasks	80 tasks	160 tasks	1645 tasks
uni-sc	68.10	70.42	n.a.	n.a.
ch-mod	89.97	87.39	81.84	60.38
Ours	96.85	95.60	95.57	88.83

materials. We used a batch size of 128 images trained on 2 GPUs with learning rate of $1e^{-4}$ using the Adam optimizer.

Figure 6b shows the training curves of our architecture and the channel modulation architecture, both with an auxiliary localization loss, on the 1645 tasks from set B, for 400 epochs, evaluated on the validation set of CLEVR every 5 epochs. The training curves show different training dynamics. Our architecture demonstrates immediate and consistent increase in the accuracy levels and asymptotically converges to higher accuracy (98.31%). The channel modulation approach repeatedly kept a low initial accuracy for over 35 epochs before increasing (with an asymptotic value of 97.32%). Training it with larger ($1e^{-3}$) or smaller ($1e^{-5}$) learning rates produced lower accuracies (dotted curves on figure 6b).

We quantified the speed of learning and its dependencies on the architecture, tasks difficulty and number of tasks by an early stopping of the training process after 100 epochs. Table 3 shows that our results are better than all other methods, both on set A (10 tasks) and set B (40 tasks), with a larger gap on set B. The larger gap is due to the difficulty of the tasks in set B, since enlarging the number of tasks to forty on set A produces a much smaller gap (up to 1.8%). The third column in the table shows the number of parameters of each architecture as a multiplier of the number of parameters in a single task VGG-11 backbone.

Table 4 shows the accuracies of gradually increasing the number of tasks up to 1645 (set B, trained for 100 epochs). Our results are scalable with the number of tasks, with a smaller decrease in performance for 1645 tasks compared

Table 5. Performance (mean \pm std of 5 repetitions) on CUB200, higher is better. Our architecture achieves better accuracies than all other methods. All models trained for 200 epochs using a resnet-18 backbone.

	loc	Av. Acc. \pm std
Single task	\times	74.34 \pm 0.07
Uniform scaling	\times	77.49 \pm 0.05
mult-obj-opt	\times	77.75 \pm 0.12
ch-mod	\times	79.87 \pm 0.14
ch-mod	\checkmark	79.91 \pm 0.18
Ours	\checkmark	80.89 \pm 0.09

with alternatives. Note that for the 1645 tasks experiment our architecture gets approximately 40 presented images per task per epoch. The uniform scaling approach cannot scale above 80 tasks due to memory restrictions. The channel modulation approach can scale, but with lower accuracies.

4.3.4. CUB 200

We used the CUB200 dataset to further demonstrate our performance on real-world images with more than ten tasks while using another type of backbone architecture (a Resnet backbone). In contrast to previous experiments, we did not aim at reducing the number of parameters (since we are using a Resnet backbone); rather we demonstrate better performance, and our built-in capability to visualize the attention maps at the end of the TD stream.

We trained all models using a Resnet-18 architecture. We used a batch size of 128 images trained on 2 GPUs with learning rate of $1e^{-4}$ using the Adam optimizer for 200 epochs. While training our architecture we add an auxiliary loss at the end of the TD stream. The target in this case is a one-hot 224x224 mask, where only a single pixel is labeled as foreground, blurred by a Gaussian kernel with a standard deviation of 3 pixels. Training one task at a time, we minimize the cross-entropy loss over the 224x224 image at the end of the TD softmax output (which encourages a small detected area) for each visible ground-truth annotated task/part. For a fair comparison we also trained another version of the channel modulation architecture with an additional regression loss, calculated by a FC layer on the top of the network, using the same ground truth annotations.

Figures 7a and 7b demonstrate the attention maps produced by our architecture in inference time. Figure 7a is an example where the predicted mask is well localized on the crown of the bird (the task) and the color is correctly predicted. Figure 7b demonstrate an error case where the breast of the bird is not well localized by the mask and as a consequence the color is wrongly predicted. More examples of interest are shown in the supplementary materials.

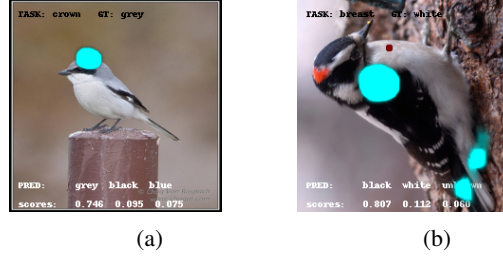


Figure 7. Visualizing the source of error; (a) good example: the crown area is well localized and the prediction follows the ground truth, (b) an error example: the breast isn't localized well enough and a black color is predicted.

Our quantitative results are summarized in Table 5. The results show better accuracy of our scheme compared to all baselines. We specifically show better accuracy compared to the channel-wise modulation scheme, indicating the preference of our image-dependent spatial-wise modulation process on the CUB200 database.

5. Summary

We described a novel architecture for multi-task learning that uses a top-down (TD) network to control the task performed by a single, non-branching bottom-up (BU) network. Ablation studies show that the tensor modification performed by the TD stream depends on the selected task, spatial location, and image content at multiple scales. We tested our network on three different datasets, showing improvements in accuracy compared with other schemes, along with scaling the number of tasks with minimal effect on performance, efficient learning in terms of data presented during learning, and helping interpretability by pointing to relevant image locations. Comparisons show higher task-selectivity of our scheme, which may explain at least in part its improved performance.

More generally, multiple-task learning algorithms are likely to become increasingly relevant, since general vision systems need to deal with a broad range of tasks, and executing them efficiently in a single network is still an open problem. Our task-dependent TD control network is a promising direction in this field in terms of accuracies and scalability. In future work we plan to adapt our described architecture to a wider range of applications (e.g. segmentation, images generation) and to a wider range of architectures with higher capacity. Our architecture is also potentially useful for problems such as online learning, domain adaptation and catastrophic forgetting and we plan to further explore these still open problems in the future.

References

- Bilen, H. and Vedaldi, A. Integrated perception with recurrent multi-task neural networks. In *Advances in neural information processing systems*, pp. 235–243, 2016.
- Cao, C., Liu, X., Yang, Y., Yu, Y., Wang, J., Wang, Z., Huang, Y., Wang, L., Huang, C., Xu, W., et al. Look and think twice: Capturing top-down visual attention with feedback convolutional neural networks. In *Proceedings of the IEEE International Conference on Computer Vision*, pp. 2956–2964, 2015.
- Carreira, J., Agrawal, P., Fragkiadaki, K., and Malik, J. Human pose estimation with iterative error feedback. In *Proceedings of the IEEE conference on computer vision and pattern recognition*, pp. 4733–4742, 2016.
- Caruana, R. Multitask learning. *Machine learning*, 28(1): 41–75, 1997.
- Chen, Z., Badrinarayanan, V., Lee, C.-Y., and Rabinovich, A. Gradnorm: Gradient normalization for adaptive loss balancing in deep multitask networks. *arXiv preprint arXiv:1711.02257*, 2017.
- Cheung, B., Terekhov, A., Chen, Y., Agrawal, P., and Olshausen, B. Superposition of many models into one. *arXiv preprint arXiv:1902.05522*, 2019.
- Collobert, R. and Weston, J. A unified architecture for natural language processing: Deep neural networks with multitask learning. In *Proceedings of the 25th international conference on Machine learning*, pp. 160–167. ACM, 2008.
- Gazzaley, A. and Nobre, A. C. Top-down modulation: bridging selective attention and working memory. *Trends in cognitive sciences*, 16(2):129–135, 2012.
- Gilbert, C. D. and Sigman, M. Brain states: top-down influences in sensory processing. *Neuron*, 54(5):677–696, 2007.
- Hashimoto, K., Xiong, C., Tsuruoka, Y., and Socher, R. A joint many-task model: Growing a neural network for multiple nlp tasks. *arXiv preprint arXiv:1611.01587*, 2016.
- He, K., Gkioxari, G., Dollár, P., and Girshick, R. Mask r-cnn. In *Proceedings of the IEEE international conference on computer vision*, pp. 2961–2969, 2017.
- Hopfinger, J. B., Buonocore, M. H., and Mangun, G. R. The neural mechanisms of top-down attentional control. *Nature neuroscience*, 3(3):284, 2000.
- Johnson, J., Hariharan, B., van der Maaten, L., Fei-Fei, L., Lawrence Zitnick, C., and Girshick, R. Clevr: A diagnostic dataset for compositional language and elementary visual reasoning. In *Proceedings of the IEEE Conference on Computer Vision and Pattern Recognition*, pp. 2901–2910, 2017.
- Kendall, A., Gal, Y., and Cipolla, R. Multi-task learning using uncertainty to weigh losses for scene geometry and semantics. In *Proceedings of the IEEE Conference on Computer Vision and Pattern Recognition*, pp. 7482–7491, 2018.
- Kirillov, A., He, K., Girshick, R., Rother, C., and Dollár, P. Panoptic segmentation. In *Proceedings of the IEEE Conference on Computer Vision and Pattern Recognition*, pp. 9404–9413, 2019.
- Kokkinos, I. Ubertnet: Training a universal convolutional neural network for low-, mid-, and high-level vision using diverse datasets and limited memory. In *Proceedings of the IEEE Conference on Computer Vision and Pattern Recognition*, pp. 6129–6138, 2017.
- Lamme, V. A., Super, H., and Spekreijse, H. Feedforward, horizontal, and feedback processing in the visual cortex. *Current opinion in neurobiology*, 8(4):529–535, 1998.
- LeCun, Y., Bottou, L., Bengio, Y., Haffner, P., et al. Gradient-based learning applied to document recognition. *Proceedings of the IEEE*, 86(11):2278–2324, 1998.
- Liu, R., Liu, C., Bai, Y., and Yuille, A. L. Clevr-ref+: Diagnosing visual reasoning with referring expressions. In *Proceedings of the IEEE Conference on Computer Vision and Pattern Recognition*, pp. 4185–4194, 2019a.
- Liu, S., Johns, E., and Davison, A. J. End-to-end multi-task learning with attention. In *Proceedings of the IEEE Conference on Computer Vision and Pattern Recognition*, pp. 1871–1880, 2019b.
- Maninis, K.-K., Radosavovic, I., and Kokkinos, I. Attentive single-tasking of multiple tasks. In *Proceedings of the IEEE Conference on Computer Vision and Pattern Recognition*, pp. 1851–1860, 2019.
- Misra, I., Shrivastava, A., Gupta, A., and Hebert, M. Cross-stitch networks for multi-task learning. In *Proceedings of the IEEE Conference on Computer Vision and Pattern Recognition*, pp. 3994–4003, 2016.
- Newell, A., Yang, K., and Deng, J. Stacked hourglass networks for human pose estimation. In *European conference on computer vision*, pp. 483–499. Springer, 2016.

- Piëch, V., Li, W., Reeke, G. N., and Gilbert, C. D. Network model of top-down influences on local gain and contextual interactions in visual cortex. *Proceedings of the National Academy of Sciences*, 110(43):E4108–E4117, 2013.
- Redmon, J. and Farhadi, A. Yolo9000: better, faster, stronger. In *Proceedings of the IEEE conference on computer vision and pattern recognition*, pp. 7263–7271, 2017.
- Ruder, S. An overview of multi-task learning in deep neural networks. *arXiv preprint arXiv:1706.05098*, 2017.
- Rusu, A. A., Rabinowitz, N. C., Desjardins, G., Soyer, H., Kirkpatrick, J., Kavukcuoglu, K., Pascanu, R., and Hadsell, R. Progressive neural networks. *arXiv preprint arXiv:1606.04671*, 2016.
- Sabour, S., Frosst, N., and Hinton, G. E. Dynamic routing between capsules. In *Advances in neural information processing systems*, pp. 3856–3866, 2017.
- Sam, D. B. and Babu, R. V. Top-down feedback for crowd counting convolutional neural network. In *Thirty-Second AAAI Conference on Artificial Intelligence*, 2018.
- Sener, O. and Koltun, V. Multi-task learning as multi-objective optimization. In *Advances in Neural Information Processing Systems*, pp. 527–538, 2018.
- Strezoski, G., van Noord, N., and Worring, M. Many task learning with task routing. *arXiv preprint arXiv:1903.12117*, 2019.
- Welinder, P., Branson, S., Mita, T., Wah, C., Schroff, F., Belongie, S., and Perona, P. Caltech-UCSD Birds 200. Technical Report CNS-TR-2010-001, California Institute of Technology, 2010.
- Zamir, A. R., Wu, T.-L., Sun, L., Shen, W. B., Shi, B. E., Malik, J., and Savarese, S. Feedback networks. In *Proceedings of the IEEE Conference on Computer Vision and Pattern Recognition*, pp. 1308–1317, 2017.
- Zanto, T. P., Rubens, M. T., Bollinger, J., and Gazzaley, A. Top-down modulation of visual feature processing: the role of the inferior frontal junction. *Neuroimage*, 53(2): 736–745, 2010.
- Zhao, X., Li, H., Shen, X., Liang, X., and Wu, Y. A modulation module for multi-task learning with applications in image retrieval. In *Proceedings of the European Conference on Computer Vision (ECCV)*, pp. 401–416, 2018.